Progress In Electromagnetics Research C, Vol. 72, 105–113, 2017

Wideband Orthogonally Polarized Resonant Cavity Antenna with Dual Layer Jerusalem Cross Partially Reflective Surface

Swati Vaid[1, *] and Ashok Mittal[2]

Abstract—A wideband orthogonally polarized resonant cavity antenna (RCA) with double-layer Jerusalem Cross type partially reflective surface (PRS) as superstrate is presented in this paper. The PRS is analyzed using equivalent circuit modelling and full wave simulations. Two-port dual-polarized aperture coupled microstrip patch has been used as primary feed antenna. Measured results show that the antenna structure exhibits 10 dB return loss bandwidth of 14.7% at 10 GHz (9.4–10.9 GHz), and the isolation between the feeding ports is better than 18 dB over the bandwidth. The cross-polarization levels in both E and H planes are better than 15 dB. The peak directivity of the antenna is 13 dBi in the entire band. The antenna is suitable for marine and weather Radar applications.

1. INTRODUCTION

Directive dual-polarized planar antennas are used in high speed wireless systems to mitigate the effect of fading due to multipath propagations. These types of antennas are also used in Radars to extract the information about target's multiple features, whereas conventional planar antennas, such as microstrip patch antenna and slot antennas, suffer from low directivity and gain because of small aperture, surface wave excitation and back lobe radiation. On the other hand, reflectors and substrates made up of artificial surfaces (i.e., Artificial Magnetic Conductors and Frequency Selective Surfaces (FSS) etc.) can be used to reduce back lobe radiation [1] or surface waves [2] and increase directivity and gain. However, the effect of back lobe radiation and surface waves on the directivity/gain performance of the antenna is less than the effect of aperture size. The aperture size of a planar antenna can be increased by using antenna array configuration or resonant cavity antenna configuration. Resonant cavity antenna (RCA) configuration consists of planar feed antenna loaded with 1-D electromagnetic bandgap structures (EBG) [3, 4], partially reflecting surfaces (PRS) or FSS [5] as superstrates. These antenna structures are simple in design and construction compared to array configuration. Further, RCAs have low loss and high gain which make them ideal for wireless and Radar applications.

Dual-polarized resonant cavity antennas for dual-band operation have been reported in the literature by using double [6] or single layer [7] PRS. Similarly, wideband dual-polarized resonant cavity antennas have also been reported with different PRS structures. In [8], wideband dual-polarized RCA was reported for 5G wireless local networks (WLANs) application. The feed antenna consisted of two orthogonal bow-tie dipoles over ground plane. The measured bandwidth was 5.3–6.3 GHz (17.2%). The gain of the antenna was 12.1 dBi at 5.5 GHz. In [9], a broadband resonant cavity antenna operating at Ka band with high gain and dual-polarization was reported. A double-sided complementary-circular patch PRS was used in the above mentioned antenna to enhance the directivity and radiation bandwidth. Further, a square patch coupled with two orthogonal slots and fed by two microstrip lines was also applied as the primary feed to achieve dual-polarization operation. The impedance bandwidth of the

Received 11 January 2017, Accepted 1 March 2017, Scheduled 16 March 2017
* Corresponding author: Swati Vaid (vaid2006@gmail.com).
[1] USICT, Guru Gobind Singh Indraprastha University, Dwarka, Delhi-78, India. [2] G.B. Pant Engineering College, Okhla, Delhi-20, India.

two ports for the reflection coefficient (S_{11}) below −10 dB was 2.5 GHz from 34 GHz to 36.5 GHz (7.1%), which covered the common 3 dB gain bandwidth of the two ports. At the center frequency of 35 GHz, the measured peak gains at the two orthogonal ports were 16.1 dBi and 15.1 dBi, respectively. The reported isolation between the two ports was higher than 30 dB within the bandwidth.

In this paper, a wideband dual-polarized RCA is reported for X-band applications. It consists of dual-layer Jerusalem cross type PRS as superstrate. This type of PRS structure has not been explored earlier for orthogonally polarized antenna application. Double-layer PRS has positive reflection phase gradient which enhances the gain of wideband orthogonally polarized patch antenna. Full wave simulations and equivalent circuit model is used to analyze the PRS. Aperture coupled square patch fed by two orthogonal microstrip lines is used as the primary feed antenna.

2. ANTENNA GEOMETRY AND DESIGN

The geometry of the proposed structure is shown in Figs. 1(a)–(b). It consists of a aperture coupled square patch antenna, feeding a leaky cavity formed between a two-layer PRS superstrate and ground plane. The RCA is designed and fabricated with 8×8 array of PRS unit cells as superstrate.

2.1. Superstrate

The PRS superstrate is formed by using two layers of 8×8 unit cells. Each unit cell consists of metallic Jerusalem cross printed on RT duroid 5880 of thickness 0.762 mm and dielectric constant 2.2 (shown in Figs. 1(a)–(b)). The dimensions of the PRS are optimized to achieve positive reflection phase gradient

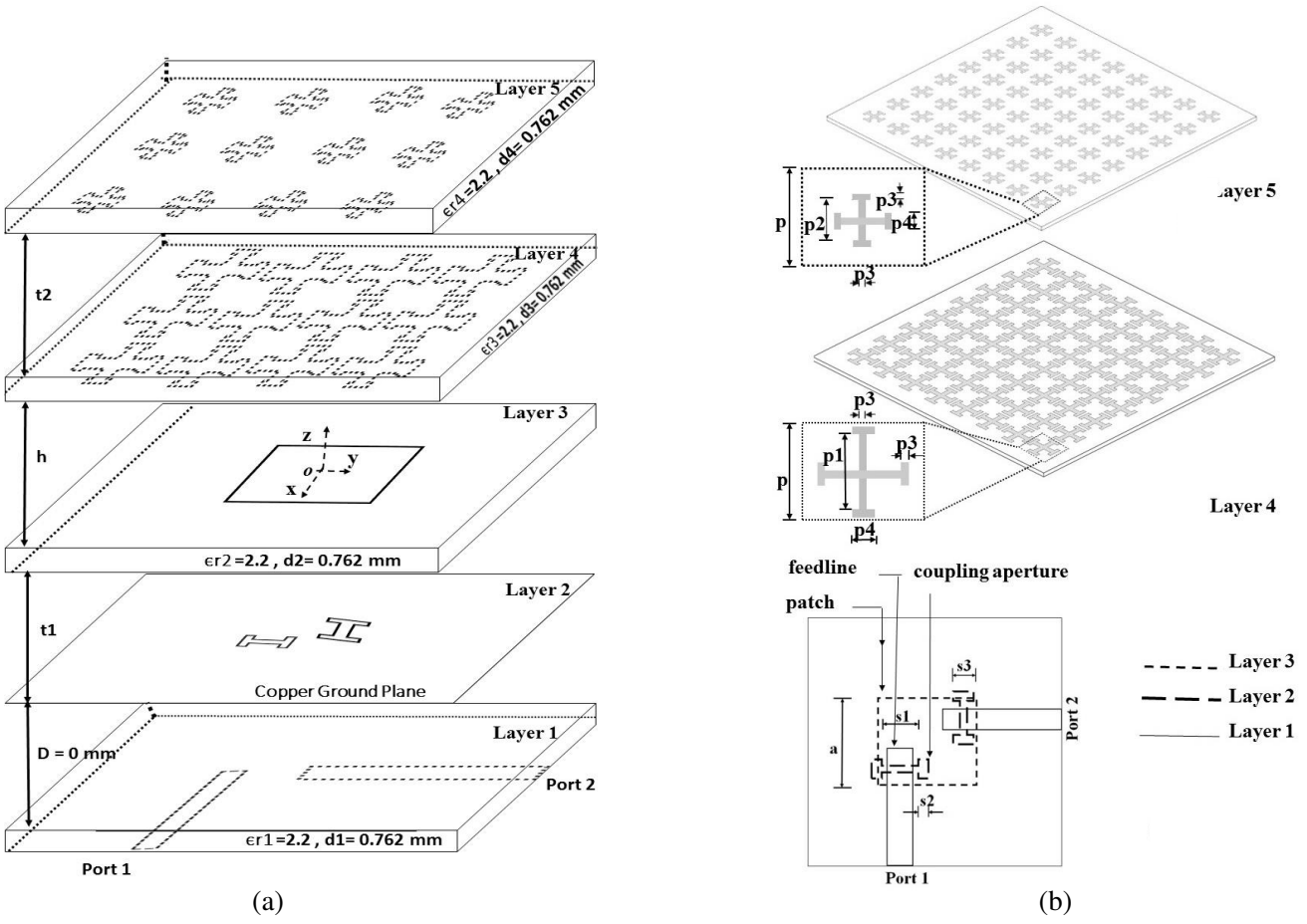

Figure 1. (a) Stacking details of the structure. (b) Dimensional details of the proposed structure.

at 10 GHz center frequency using CST software. The periodicities of the unit cells are kept the same in both the PRS layers (Layer 4–5), i.e., 6.5 mm each, but the sizes of crosses on the two layers are unequal. The height between the two PRS layers t_2 is kept as 3 mm to tune the reflection phase characteristics of PRS for 10 GHz center frequency. The optimized dimensions of metallic crosses are with $p1 = 5$ mm, $p2 = 4.5$ mm, $p3 = 0.5$ mm, $p4 = 1.5$ mm.

2.2. Feed Antenna

An aperture-coupled patch antenna resonates if the following condition is satisfied,

$$n_1^2 B_{\text{Patch}} + B_{\text{ap}} = 0 \tag{1}$$

where, B_{patch} and B_{ap} are the susceptances of patch and H-shaped slot, respectively. n_1 represents coupling of the patch to the aperture and is roughly equal to fraction of patch current intercepted by slot to the total patch current. When being excited by electrically small slot, the imaginary part of the patch admittance cancels with slot inductance at resonance. A complete analysis of aperture coupled patch antenna is given in [10].

In the present work, an aperture-coupled square patch antenna is designed at the frequency of 10 GHz with patch dimensions of 9 mm × 9 mm ('a' × 'a') on RT duroid 5880 with thickness ($h_2 = 0.762$ mm). H-shaped coupling apertures in the ground plane are used to feed the patch for improved coupling between microstrip feedline and patch. The dimensions of the apertures are $s_1 = 3.18$ mm, $s_2 = 1.48$ mm and $s_3 = 2.52$ mm.

The apertures are positioned at a distance of 2.5 mm from the center of the patch for best impedance matching. Air gap of $t_1 = 2$ mm is maintained between the substrate of the feedlines and patch substrate. The air gap reduces the effective dielectric constant of the medium on which patch antenna is placed, reducing the quality factor of the patch antenna and increasing its bandwidth.

2.3. Composite Structure

The stacking details of the composite structure are shown in Fig. 1(a). An air gap of height 'h' = 15 mm is maintained between the PRS superstrate and aperture-coupled square patch antenna by using Teflon spacers. The lateral dimension of the composite antenna is $2\lambda_0 \times 2\lambda_0$ (where λ_0 corresponds to the center frequency of 10 GHz) with total height equal to $t_1 + h + t_2 = 20$ mm.

3. PRS ANALYSIS

In the present work, PRS is formed by printing capacitive Jerusalem cross type frequency selective surfaces (FSS) on two dielectric layers separated by distance $t_2 = 3$ mm. The FSS is analyzed by full wave simulations on CST STUDIO SUITE for normal incidence. The L-C parameters of the PRS are extracted by fitting the values of parameters in the circuit (shown in Fig. 2) using ADS optimisation tool. The S parameters of the PRS obtained by using CST are taken as the goal function for optimisation. Reflection magnitude and phase of the PRS at 1000 frequency points in the frequency range of 6–12 GHz is considered as goal.

The impedance of single-layer Jerusalem cross type frequency selective surface is given by the following expression [11],

$$Z_J = \frac{\left(1 - \omega^2 L_{s1} C_{s1}\right)\left(1 - \omega^2 L_{s2} C_{s2}\right)}{j\omega\left(C_{s1} + C_{s2} - \omega^2 C_{s1} C_{s2}\left(L_{s1} + L_{s2}\right)\right)} \tag{2}$$

Circuit model of the proposed two-layer PRS is shown in Fig. 2. Series combinations of 'L_{s1}', 'C_{s1}' and 'L_{s2}', 'C_{s2}' in the circuit represent Jerusalem crosses on Layer 4 of the design. Series combinations of 'L'_{s3}, 'C_{s3}' and 'L_{s4}', 'C_{s4}' are used for crosses on Layer 5. Z_0 shows the wave impedance in air. The transmission line sections between series networks of circuit elements represent dielectric layers upon which the metal patterns of PRS layers are printed with impedances equal to Z_a, Z_c (i.e., wave impedance in the dielectric) and corresponding lengths equal to d_a and d_c, whereas Z_b (i.e., wave impedance in air) represents the air gap between two PRS layers. The optimized values of the parameters

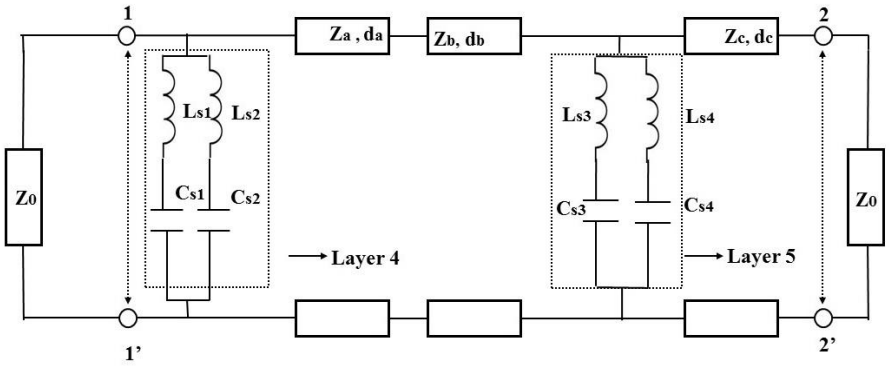

Figure 2. Equivalent circuit of PRS.

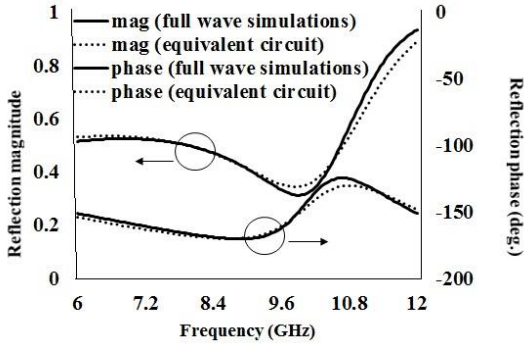

Figure 3. Reflection characteristics of PRS.

obtained from ADS are $L_{s1} = 2.85\,\text{nH}$, $C_{s1} = 0.044\,\text{pF}$, $L_{s2} = 0.017\,\text{nH}$, $C_{s2} = 0.009\,\text{pF}$, $L_{s3} = 0.31\,\text{nH}$, $C_{s3} = 0.047\,\text{pF}$, $L_{s4} = 0.032\,\text{nH}$, $C_{s4} = 0.0036\,\text{pF}$ and $Z_a = Z_c = 254\,\Omega$.

The S parameters obtained from full wave simulations using CST STUDIO SUITE for the PRS are compared with the equivalent circuit S parameters obtained using ADS. Fig. 3 shows the computed and simulated graphs of the reflection magnitude and reflection phase of the PRS at port 1. It can be seen from the figure that the PRS has positive reflection phase gradient. The reflection phase plays an important role in deciding the height at which PRS needs to be placed, above the feeding antenna to get desired resonance [12]. To achieve wide impedance bandwidth and low sidelobes in the radiation pattern, the PRS is placed at a height of 15 mm (which is half a wavelength at the centre frequency of 10 GHz) from the patch.

4. PARAMETRIC ANALYSIS

4.1. PRS

4.1.1. Variation of t2

By varying the height between the two FSS layers, the center frequency of the positive reflection phase gradient can be tuned. Fig. 4(a) shows the effect of changing $t2$ from 2.5 mm to 3.5 mm on the reflection characteristics of the PRS. Increasing $t2$ lowers the center frequency of positive reflection phase gradient.

4.1.2. Variation of p4

The center frequency of the positive reflection phase gradient can also be tuned by varying length $p4$ of the Jerusalem crosses of FSS layers. Fig. 4(b) shows the effect of changing $p4$ from 1 mm to 2 mm on the reflection characteristics of the PRS. Increasing $p4$ lowers the center frequency of positive reflection phase gradient.

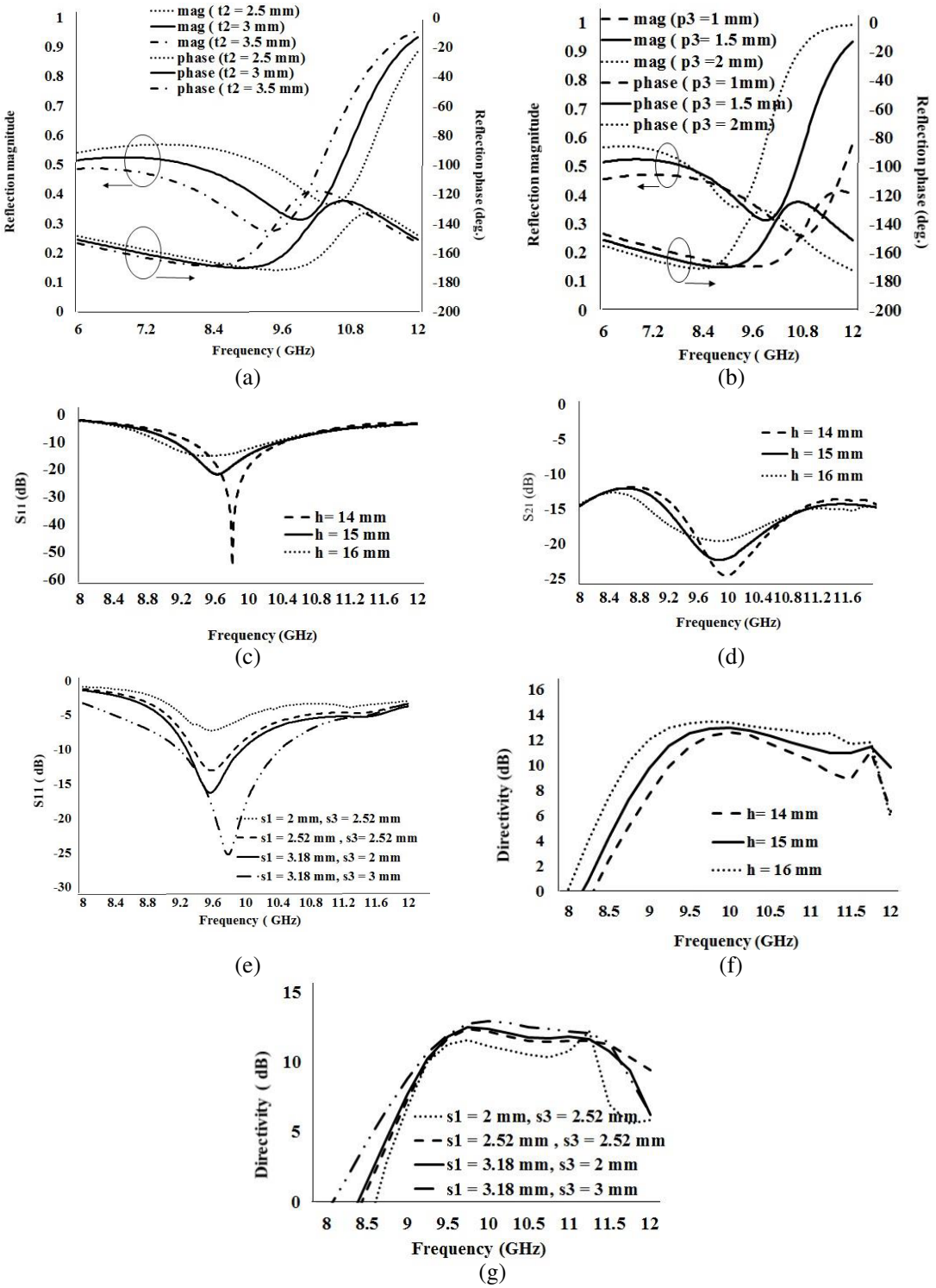

Figure 4. (a) Variation in reflection magnitude and phase of PRS by varying $t2$. (b) Variation in reflection magnitude and phase of PRS by changing $p4$. (c) Effect of cavity height variation on S_{11} of RCA configuration. (d) Effect of cavity height variation on S_{21} of RCA configuration. (e) Effect of variation in the dimensions of H shaped apertures on S_{11} of RCA configuration. (f) Effect of cavity height variation on the directivity of RCA configuration. (g) Effect of variation in apertures dimensions on the directivity of RCA configuration.

4.2. RCA

Parametric effectd of cavity height 'h' and H-shaped aperture dimensions ('$s1$' and '$s3$') on the reflection characteristics and directivity of the RCA have been studied.

4.2.1. Reflection Characteristics

When cavity height 'h' is varied from 14 to 16 mm, there is a shift of 0.2 GHz in the 10 dB return loss bandwidth, as shown in Fig. 4(c). The frequency range shifts down with increasing height, whereas the impedance matching improves over the bandwidth. Fig. 4(d) shows a graph of port isolation (S_{21}) versus frequency. It is observed that the effect of h variation on S_{21} is the same as on S_{11}.

The dimensions of H-shaped apertures affect the coupling between feedlines and patch antenna. Fig. 4(e) shows the effect of variation in aperture dimensions on reflection coefficient of antenna. The excitation is applied at port 1, and port 2 is match terminated.

4.2.2. Directivity

Figure 4(f) shows the variation in directivity (RCA is fed at port 1) when cavity height is varied from 14 to 16 mm. It is observed that increase in height h increases the 3 dB directivity bandwidth of the RCA by up to 1.2 GHz. Peak directivity also increases by 1 dB with the increase in height. The increase in peak directivity is because of the improved matching with the increase in h. Fig. 4(g) shows the effect of varying aperture dimensions on the directivity of the antenna.

5. EXPERIMENTAL RESULTS AND DISCUSSION

The proposed structure is fabricated and tested. The S parameters of the RCA are measured using Anritsu MS2038C VNA Master. Figs. 5(a)–(b) show the reflection coefficients (S_{11} and S_{22}) of the proposed RCA configuration with 8×8 array of PRS unit cells, obtained at ports 1 and 2 with the

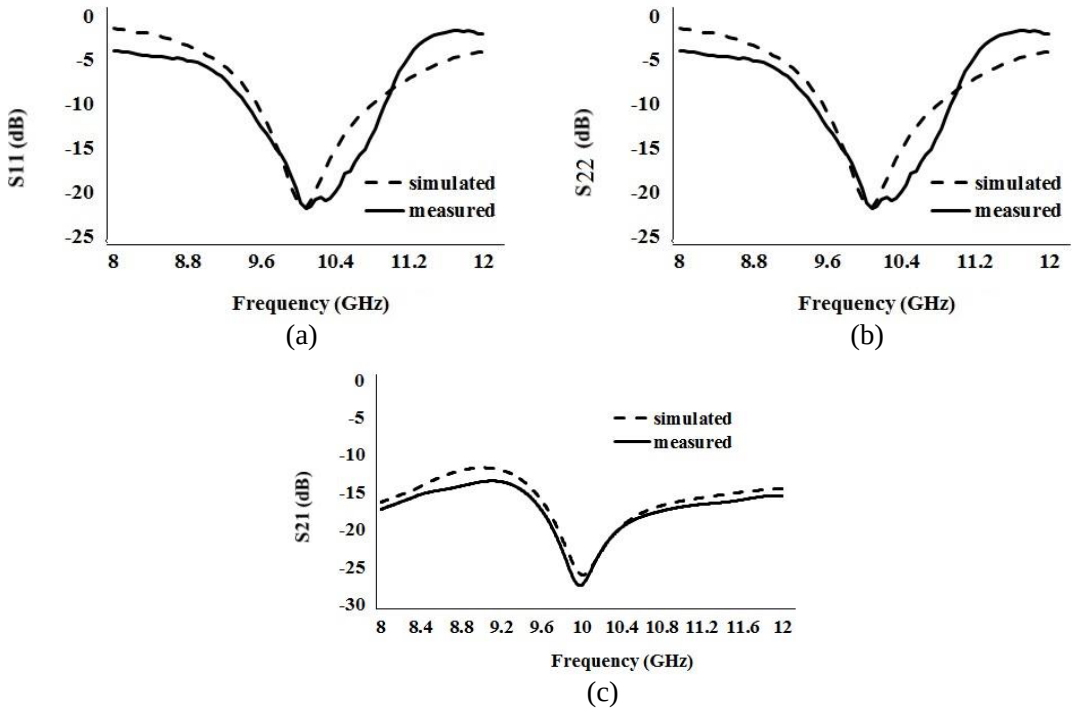

Figure 5. (a) Return Loss at port 1. (b) Return Loss at port 2. (c) Isolation between port 1 and port 2.

other port match terminated. The measured results are in close agreement with the simulated ones. The measured 10 dB return loss bandwidth of the RCA is 14.7% at 10 GHz (9.4–10.9 GHz). Fig. 5(c) shows the isolation (S_{21}) between the two feeding ports. The two feeding ports for orthogonal polarization (Vertical (V) and Horizontal (H)) are very much in isolation. Isolation more than 18 dB is obtained for the frequency range 9.4–10.9 GHz.

Figure 6(a)–(d) show the measured antenna gain pattern in $\Phi = 0°$ (xoz), $\Phi = 90°$ (yoz) planes and cross polarization levels at 9.5 GHz and 10 GHz, when being fed via port 1. It was ensured that port 2 was match terminated. The antenna radiation patterns in both the principal planes are measured using in-house antenna measurement facility (in an Anechoic Chamber). The measured gains of the antenna are 10.5 dBi and 10 dBi at 9.5 GHz and 10 GHz. The cross-polarization level is less than 15 dB.

The bore-sight directivity of the feed antenna (patch) used in the proposed configuration is compared with the directivity of the composite structure (i.e., feed antenna loaded with PRS) (when being fed at port 1) and is shown in Fig. 7, for the entire operating band from 8–12 GHz. It can be seen

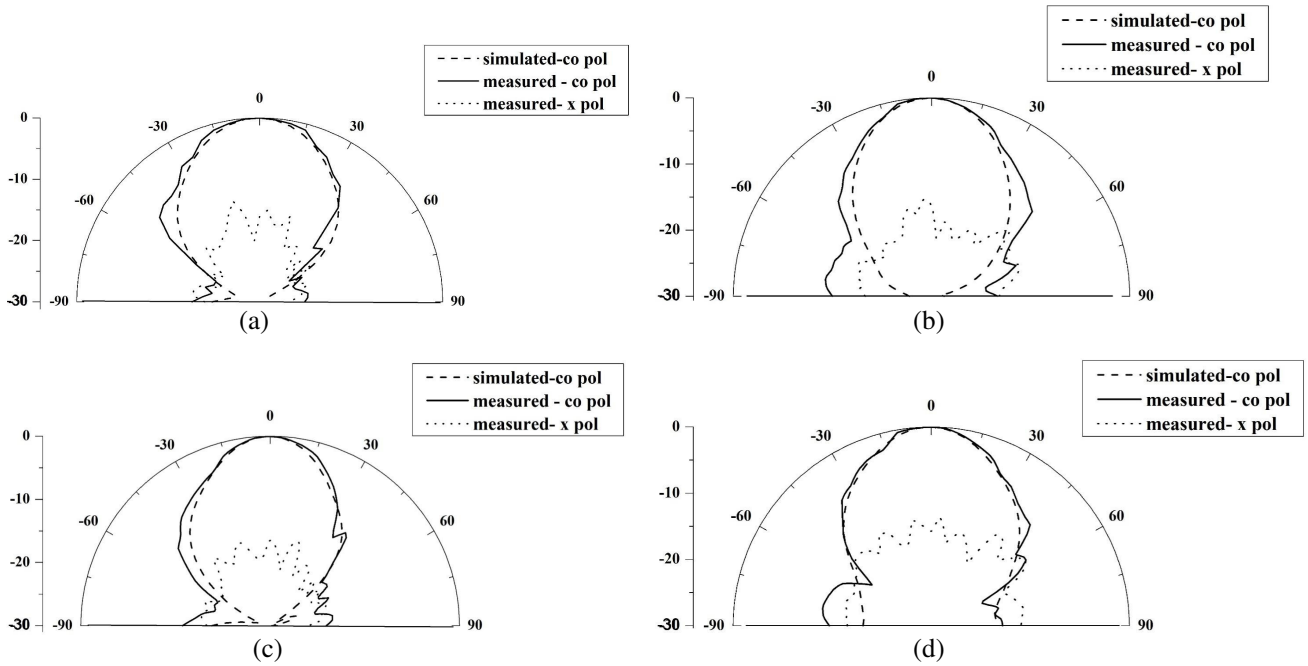

Figure 6. (a) Simulated and measured normalized radiation pattern at 9.5 GHz ($\Phi = 0°$), fed at port 1. (b) Simulated and measured normalized radiation pattern at 9.5 GHz ($\Phi = 90°$), fed at port 1. (c) Simulated and measured normalized radiation pattern at 10 GHz ($\Phi = 0°$), fed at port 1. (d) Simulated and measured normalized radiation pattern at 10 GHz ($\Phi = 90°$), fed at port 1.

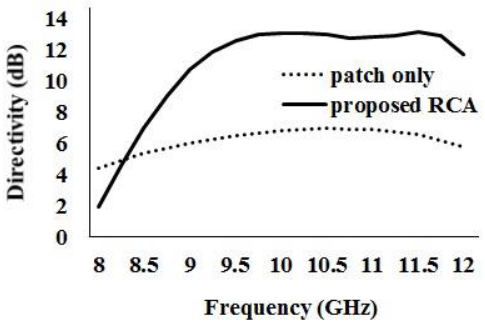

Figure 7. Simulated directivity versus frequency for the RCA configuration.

that there is 6 dB enhancements in the bore-sight directivity of the antenna in the entire band with the PRS.

Comparison of the proposed model with the RCA models reported earlier in the literature is given in Table 1.

Table 1. Comparison with reported models.

References	Return Loss Bandwidth (%)	Peak Directivity (dB)	Peak Realized Gain (dB)	Isolation (dB)	Relative Size (λ w.r.t. center frequency)	FSS Type
[8]	17.2	-	12.1	-	$2\lambda \times 2\lambda \times 0.68\lambda$	Single layer, single sided
[9]	7.1	-	15.1, 16.1	> 30	$3\lambda \times 3\lambda \times 0.66\lambda$	Single layer, Double sided
Present work	14.7	13	10.5	> 18	$2\lambda \times 2\lambda \times 0.66\lambda$	Double Layer

6. CONCLUSION

The design of a wideband orthogonally polarized resonant cavity antenna with double-layer Jerusalem cross type partially reflective surface (PRS) as superstrate is presented in this paper. Full wave simulations and equivalent circuit model is used to understand the electromagnetic behavior of PRS. The structure exhibits 10 dB return loss bandwidth of 14.7% and isolation more than 18 dB. Peak realized gain and directivity of the antenna structure are 10.5 and 13 dBi respectively in the entire bandwidth. Comparison with earlier reported designs is presented.

REFERENCES

1. Mohamad, S., R. Cahill, and V. Fusco, "Performance of Archimedean spiral antenna backed by FSS reflector," *Electronics Letters*, Vol. 51, No. 1, 14–16, 2014.
2. Gonzalo, R., P. De Maagt, and M. Sorolla, "Enhanced patch-antenna performance by suppressing surface waves using photonic-bandgap substrates," *IEEE Transactions on Microwave Theory and Techniques*, Vol. 47, No. 11, 2131–2138, 1999.
3. Weily, A. R., K. P. Esselle, T. S. Bird, and B. C. Sanders, "High gain circularly polarised 1-D EBG resonator antenna," *Electronics Letters*, Vol. 42, No. 18, 1012–1014, 2006.
4. Zeb, B. A. and K. P. Esselle, "High-gain dual-band dual-polarised electromagnetic band gap resonator antenna with an all-dielectric superstructure," *IET Microwaves, Antennas & Propagation*, Vol. 9, No. 10, 1059–1065, 2015.
5. Feresidis, A. P. and J. C. Vardaxoglou, "High gain planar antenna using optimised partially reflective surfaces," *IEE Proceedings — Microwaves, Antennas and Propagation*, Vol. 148, No. 6, 345–350, 2001.
6. Moghadas, H., M. Daneshmand, and P. Mousavi, "A dual-band high-gain resonant cavity antenna with orthogonal polarizations," *IEEE Antennas and Wireless Propagation Letters*, Vol. 10, 1220–1223, 2011.
7. Moghadas, H., M. Daneshmand, and P. Mousavi, "Dual-band high-gain resonant cavity antenna with orthogonal polarisation using slotted patch partially reflective superstrate," *Electronics Letters*, Vol. 48, No. 15, 897–899, 2012.
8. Zhu, H., Y. Yu, X. Li, and B. Ai, "A wideband and high gain dual-polarized antenna design by a frequency-selective surface for WLAN application," *Progress In Electromagnetics Research C*, Vol. 54, 57–66, 2014.

9. Tan, G.-N., X.-X. Yang, H.-G. Xue, and Z. Lu, "A dual-polarized Fabry-Perot cavity antenna at Ka band with broadband and high gain," *Progress In Electromagnetics Research C*, Vol. 60, 179–186, 2015.
10. Garg, R., *Microstrip Antenna Design Handbook*, Artech House, 2001.
11. Costa, F., A. Monorchio, and G. Manara, "Efficient analysis of frequency-selective surfaces by a simple equivalent-circuit model," *IEEE Antennas Propag. Magazine*, Vol. 54, 35–48, 2012.
12. Von Trentini, G., "Partially reflecting sheet arrays," *IRE Trans. Antennas Propag.*, Vol. 4, 666–671, 1956.